Effect of High Electronic Current Density on the Motion of Au^{195} and Sb^{125} in Gold*†

H. MICHAEL GILDER‡ AND DAVID LAZARUS
Department of Physics and Materials Research Laboratory, University of Illinois, Urbana, Illinois
(Received 25 August 1965; revised manuscript received 17 January 1966)

The effect of high electronic current density on the motion of the Au^{195} and Sb^{125} ions in gold was studied by means of a novel lathe-sectioning technique that permitted the assay of radioactive sections from a specimen only 3 mm in diameter. The mobility v/j of the Au^{195} ion in gold was investigated in the temperature range 874 to 1016°C, with a corresponding variation in mobility of from 9.6×10^{-13} to 7.3×10^{-12} cm³/A sec, and was found, within experimental uncertainty, to obey the Nernst-Einstein relation, $v/j=e^*\rho D/kT$. The effective charge e^* was determined to be independent of temperature, with the value $(9\pm1)e$, indicating that momentum exchange with the conduction electrons dominates the force arising from the direct interaction between the external electric field and the positively charged ion. The specific resistivity of the gold ion-vacancy complex was calculated to be (1.2 ± 0.3) $\mu\Omega$cm/(% defect). The electromigration of the Sb^{125} ion in gold was studied at a temperature of 853°C, for which the mobility was 9.24×10^{-11} cm³/A sec, and at 1009°C, corresponding to a mobility of 4.54×10^{-10} cm³/A sec. The effective charge and specific resistivity of the activated complex are $(140\pm40)e$ and (18 ± 6) $\mu\Omega$ cm/(% defect), respectively. As the shift of the Sb^{125} tracer was some 50% greater than the mean-square diffusional penetration distance of the antimony, and the mobility of the antimony ion some one to two orders of magnitude greater than that of the solvent gold atoms, it appears that electromigration techniques could be adapted as a practical method for purifying metals, as an addition to, or substitute for, zone refinement.

I. INTRODUCTION

THE drift of charged ions under an electric field in liquids or in solids at high temperatures is, of course, a familiar phenomenon associated with ionic conductivity. Much less familiar is the recently discovered ionic drift in solid or liquid metals—a phenomenon usually termed *electromigration*. In metals, the electric current is carried by mobile electrons, so that only extremely small electrostatic fields can be applied across a metal sample. Still, there is strong evidence that ionic motion occurs in metals, both in liquids and in solids, at high temperatures.

The first evidence for electromigration in solids was found in studies of interstitial alloys. When a large current is passed through iron containing dissolved carbon at high temperatures, the carbon atoms drift toward the cathode, as though they were mobile positive charges.[1] From the measured mobility and electric field, it is possible to deduce an effective "ionic charge" for the carbon atoms. Similar effects have been noted for substitutional alloys,[2] where electromigration results in segregation of the constituents. In some systems, however, atoms apparently move in the wrong direction; ostensibly positive ions move toward the anode.[2] The effects therefore, clearly cannot be explained solely as the drift of a clearly defined ionic charge in an electrostatic field. Instead, two effects must be considered: Ions may drift in the applied external field, but, in addition, they may be forced in one direction or the other by direct collisions with the moving charge carriers. Thus, if the predominant charge carriers were electrons, such collisions would drive atoms toward the anode, while, for holes, the motion would be toward the cathode.

The problem has been treated semiclassically by Fiks,[3] Huntington and Grone,[4] Bosvieux and Friedel,[5] and others.[6,7] In Fiks's formulation, we consider that the total force on an impurity ion in a conducting medium is given by

$$F=\alpha ez\epsilon(1-\Delta\rho_0/c\rho), \qquad (1)$$

where ϵ is the external electric field, α the excess valence of the impurity, z the electron-atom ratio, e the electronic charge, $\Delta\rho_0$ the residual resistivity associated with the impurity, c the atomic fraction of impurities, and ρ the bulk resistivity of the solvent.

Evidence has also been found for electromigration in pure metals, although the effects are much smaller than observed in alloys.[2] Equation (1) may still be used to describe the driving force by considering the saddle-point configuration corresponding to a vacancy or interstitial exchange to be equivalent to an impurity ion, with the excess specific resistivity of the activated complex being analogous to the quantity $\Delta\rho_0$ and c then being the concentration of activated complexes. Fiks's expression for the force on an impurity ion is then essentially equivalent to the following expression derived by Huntington for the force on a diffusing ion in a pure metal:

$$f=e\epsilon z[1-\tfrac{1}{2}(\rho_d N/\rho N_d)|m/m^*|]=e^*\epsilon, \qquad (2)$$

* This work was supported in part by the U. S. Atomic Energy Commission under Contract AEC (11-1)-1198.
† This paper is based on a thesis submitted by H. M. Gilder to the Graduate College of the University of Illinois in partial fulfillment of the requirements for the Ph.D. degree.
‡ Present address: Department of Physics, Rensselaer Polytechnic Institute, Troy, New York.
[1] P. Dayal and L. Darken, Trans. AIME **188**, 1156 (1960).
[2] H. Wever and W. Seith, Z. Elektrochem. **59**, 942 (1955); W. Seith and H. Etzold, *ibid.* **40**, 829 (1934).
[3] V. B. Fiks, Fiz. Tverd. Tela **1**, 16 (1959) [English transl.: Soviet Phys.—Solid State **1**, 14 (1959)].
[4] H. B. Huntington and A. R. Grone, J. Phys. Chem. Solids **20**, 76 (1961).
[5] C. Bosvieux and J. Friedel, J. Phys. Chem. Solids **23**, 123 (1962).
[6] B. Baranowski, Bull. Acad. Polon. Sci. **3**, 117 (1955).
[7] P. C. Mangelsdorf, Jr., J. Chem. Phys. **33**, 1151 (1960).

where ρ_d is the defect resistivity, N_d the density of defects, N the density of metallic ions, m the free electronic mass, m^* the effective electronic mass, and e^* the effective ionic charge. Although the force on the ion is not directly measurable, it can be estimated experimentally by measuring the drift velocity $\mathbf{v}$ of the ions and the diffusion coefficient appropriate to their motion, as well. The Nernst-Einstein relation

$$\mathbf{v}=D\mathbf{F}/kT, \tag{3}$$

where k is Boltzmann's constant, then connects the observable quantities with the ionic force.

Two different methods have been used for the study of electromigration in pure metals. In one, the motion of surface scratches is followed as a function of time. The scratches are assumed to be markers fixed to the lattice, and the effect is detected by the motion of markers in the hot zone relative to a marker in the cold part of the specimen. Using this technique, measurements have been made of electromigration in pure gold,[4] aluminum,[8] indium,[9] copper,[10] and other metals.[11] The second method, developed by Kuzmenko and coworkers,[12] employs a radioactive-tracer technique. Tracers are deposited at the end of a cylindrical specimen which is then placed in contact with a second rod, and a current passed through the combination. After diffusion, the welded interface is broken apart, and the motion of the tracer relative to weld is determined by sectioning. A wide variety of metals have been studied in this fashion.

Unfortunately, there are glaring discrepancies between the results found by the two different techniques, and each is subject to possibly large systematic errors. In gold, for example, the "ionic" mobility reported by Kuzmenko with the tracer method was sixteen times larger than that found by Huntington and Grone, and a factor of 6 greater than that obtained by Grone for copper by use of the surface-marker technique. The use of surface scratches as markers suffers from two obvious problems: first, there is lattice distortion in the vicinity of the scratch marks due to the creation of atomic planes on one side and the annihilation of planes on the other; secondly, since the drift depends on dimensional changes between the surface marker and a fiducial marker in the cold region of the specimen, the measured drift is subject to corrections[8] involving the longitudinal and lateral strains arising from the mass flow. Kuzmenko's technique also involves possibly large errors, since the welded couple must be broken open after electromigration is completed. If the weld, after diffusion, were so porous and brittle that it could be broken open easily, then the temperature and current distributions at the weld, during diffusion, are probably quite different from those measured in the bulk. Alternatively, if the weld formed were mechanically and electrically sound, then considerable distortion of the specimen could occur when it is broken open, so that the geometry of the broken specimen, near the interface, may be quite different from that of the undistorted welded couple.

In the present experiment the mobilities of Au^{195} and, as a typical impurity Sb^{125}, were measured by a new tracer method which overcomes the objections of both earlier techniques. Motion is measured with respect to inert $Hf^{181}O_2$ markers placed initially at a welded interface,[13] so that there are no errors due to lattice distortion. In addition, the use of internal markers ensures isothermal conditions in the region of diffusion. The specimen is welded soundly together before electromigration, and subsequently sectioned completely through, avoiding any distortion associated with breaking open the interface.

The electromigration effect can be viewed as a biased random walk under the action of an external force field which raises the effective barrier for diffusional jumping in one direction and lowers the barrier in the opposite direction. In the presence of the external force, the diffusion equation can be written as

$$\partial n/\partial t=D\partial^2 n/\partial x^2-v\partial n/\partial x, \tag{4}$$

where

$$v=2\Delta V D/\lambda kT. \tag{5}$$

Here n is the concentration of the diffusing species, ΔV the perturbation in barrier height due to the force field, λ the jump distance, and D the appropriate diffusion coefficient. If Eq. (4) is solved for n with the boundary condition that at $t=0$, $n=n_0e^{-x^2/x_w^2}$, where x_w is the distance characteristic of the interdiffusion of the tracer which occurred during the welding period, the result is

$$n(x,t)=\tfrac{1}{2}N_0(\pi Dt)^{1/2}e^{-(x-vt)^2/(4Dt+x_w^2)}. \tag{6}$$

Here N_0 is the total number of radioactive atoms, and t is time of electromigration. This solution is merely a Gaussian distribution translated from $x=0$, at a velocity v, by an amount $\Delta x=vt$.

In the present experiment, values of D and v can be determined directly from measurement of the distribution of the tracer following diffusion at high temperature under a fixed current for a known period of time. From these results, values can be deduced for the change in barrier height ΔV, the effective charge of the diffusing ion e^*, and of the specific resistivity of the diffusing complex.

II. EXPERIMENTAL PROCEDURE

A. Electromigration Apparatus and Procedure

The primary criterion in the design of the sample chamber was the creation of environmental conditions

[8] R. V. Penney, J. Phys. Chem. Solids **25**, 335 (1965).
[9] A. Lodding, J. Phys. Chem. Solids **26**, 143 (1965).
[10] A. R. Grone, J. Phys. Chem. Solids **20**, 88 (1961).
[11] H. B. Huntington and S. C. Ho, J. Phys. Soc. Japan **18** (1963).
[12] P. P. Kuzmenko, Ukr. Fiz. Zh. **7**, 117 (1962).
[13] R. Meyer and L. Slifkin (to be published).

such that maximum current densities could be sustained by the specimens in the temperature range 850 to 1050°C. To this end, massive copper electrodes, to which the specimen was attached, and the walls of the chamber were water cooled, as shown schematically in Fig. 1. In addition, the chamber was filled with helium at a positive pressure of 10 psi, circulated throughout the volume and directed against the specimen by a high-capacity, variable-speed fan. The combination of thermal conduction to the water-cooled supports and forced convection cooling by the helium gas permitted attainment of current densities of about 9.3×10^3 A/cm^2 in the gold rods without melting.

So that no physical distortion of the specimens would occur, they had to be installed and run in a stress-free condition. A special assembly was used to fulfill these requirements. One end of the gold rod was secured in a phosphor bronze draw-in lathe-collet type receptacle, housed in a copper end support fixed to one of the massive electrodes. The collet itself not only ensured good electrical and thermal contact but application of only radial forces on the rod during the mounting operation. The other end of the specimen was secured by an identical collet, housed, however, in a copper block attached to a stainless steel shaft. The shaft was constrained by precision linear bearings to one-dimensional motion parallel to the center-line of the specimen, while electrical contact was effected by having the bottom portion of the copper block contact oil-covered mercury situated in a reservoir fixed to the other electrode. This arrangement not only allowed for stress-free thermal expansion of the gold rod, but eliminated bending moments in the central region of the rod as well. Such torques, noticed initially in trial runs with free-end supports floating in mercury, consistently caused permanent distortion if not complete tearing of the central portion of the specimen. The specimen rod was carefully positioned coaxially in the mount, with the central weld placed equidistant from the end supports so that the diffusion zone was at the maximum, gradient-free portion of the temperature distribution.

With the large amount of heat drawn from the mounted specimen rod in the chamber, the temperature varied extremely rapidly with current above a critical value. Typically, the temperature of the rod, if not controlled, could vary from 750°C to the melting point, when the current changed from 650 to 660 A. To achieve stable operation for extended periods of time at high temperatures, a special control was required. The primary temperature sensing was accomplished through an electro-optical system. As shown in Fig. 1, the top plate of the chamber supported a traveling microscope focused on the specimen through an O-ring sealed Lucite window. The standard eyepiece of the microscope was replaced with a two-way eyepiece, one leg of which could be used for visual inspection of the specimen, while the other housed a *p-n* junction photo-

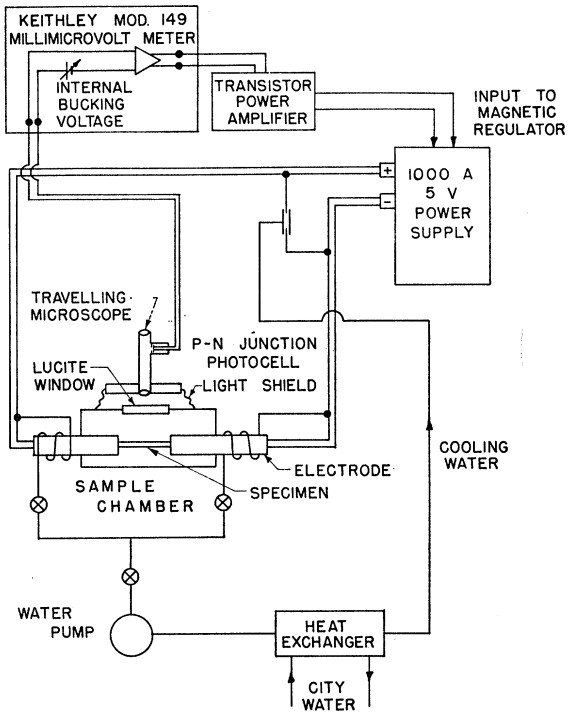

FIG. 1. Schematic diagram of apparatus.

voltaic cell. The cell output, related to the light output from a 1-mm-wide rectangular portion of the central region of the rod, was fed to a Keithley millimicrovoltmeter, used as a potentiometer with an internal bucking voltage, as shown in Fig. 1. The amplified output was further amplified by a transistor power amplifier and the final output fed to the magnetic regulator of a special 1000-A (max) 5-V (max) dc power supply. This feedback system permitted maintaining the specimen temperature constant within limits of ±5°C about the set temperature; while the current varied by about 1% in runs where there was no systematic change of current with time. In some runs, the current required to maintain constant temperature increased systematically with time, presumably due to changes in the resistance of the specimen. A continuous record of the specimen current was kept by means of a strip-chart recorder and standard shunt, so that a time-average value of the current could be ascertained. Temperature fluctuations were also continuously monitored with a micro-optical pyrometer.

B. Materials and Specimen Fabrication

All gold used was nominally 99.97% pure. The gold was vacuum cast in pure graphite crucibles into the form of nearly single-crystal cylinders about $\frac{5}{8}$ in. in diameter, and then spark-cut into $\frac{1}{4}$-in.-thick disks. One end of each disk was lapped to an optical flat ($\frac{1}{2}$ fringe or better) and very thin layers of the appropriate tracers were deposited on mating surfaces.

TABLE I. Experimental results for electromigration of Au^{195} in gold.

Run No.	Shift, Δx (μ)	Current, I (A)	Temp., T (°C)	Time, t (sec)	Diff. coeff., D (cm^2/sec)
1	42±5	670±6	995±2	6.467×10^4	5.68×10^{-9}
2	26±2	629±6	1007±2	5.435×10^4	6.60×10^{-9}
3	36±1	685±4	1016±2	5.420×10^4	7.46×10^{-9}
4	89±3	653±3	919±2	5.181×10^5	1.98×10^{-9}
5	89±3	641±6	874±2	1.050×10^6	9.78×10^{-10}

Three radioactive isotopes were employed: 185-day Au^{195}, to permit determination of the effects of the electron current on self-diffusion of the solvent; 46-day Hf^{181}, to serve as an inert marker fixed at the initial interface; and 3-year Sb^{125}, to study the effects on diffusion of a typical impurity. The tracer solutions, as received in 2 mCi units, were diluted with pure, triple-distilled water and appropriate salts to about 500 ml total volume. The Au^{195} and Sb^{125} tracer layers could be deposited in uniform thin layers (approximately 100 Å) by electroplating with a platinum anode, the Au from a standard cyanide solution, and the Sb from an oxalate solution. The Hf tracer, however, could not be electroplated. A different procedure was employed to realize uniform, sufficiently thin layers (0.03–0.05 atom layers) to ensure a sound weld. The $HfOCl_2$ in HCl, as received, was diluted with pure water, and deposited directly onto the gold optical flat with a glass eye dropper, utilizing the surface tension between the solution and the glass to "drag" the droplet over the gold surface, which was simultaneously heated by means of an infrared lamp. The heat served to evaporate the HCl and water from the specimen. Concentrated HNO_3 was then "painted" on the surface to oxidize the $HfOCl_2$ to $Hf^{181}O_2$. This procedure resulted in extremely uniform marker deposits, as ascertained by contact autoradiographs.

Mating disks were then placed with the tracer layers in contact and positioned in a special welding apparatus. The welding rig was placed in an evacuated vertical tube furnace, and an axial force corresponding to approximately twice the yield stress of gold was applied through an external screw-spring arrangement, when an equilibrium temperature of approximately 950°C was reached. Such a stress was found necessary to bring the mating surfaces into intimate contact and effect a secure weld. The stress and temperature were maintained constant for an effective time of about $1\frac{1}{2}$ hours, which gave an inter-diffusion penetration depth for the gold tracer of about 70 μ. A spark cutter was then employed to relieve nine cylindrical specimens from the original welded cylinder, with axes perpendicular to and bisected by the weld plane, all nominally 3 mm in diameter and $\frac{1}{2}$ in. long. These stubs were cast into holders and threaded at their ends, with bushings and extender rods fitted to give an over-all length of about 2 in. appropriate to the electrode gap.

C. Sectioning Procedure

After a specimen was run for a time appropriate to obtain a measurable shift (15 h to 12 days at the highest and lowest temperatures, respectively, for Au^{195} in Au, and 6 to 24 h at the highest and lowest temperatures, respectively, for Sb^{125} in Au), an epoxy cylinder was cast around and coaxial with the rod. This was done to give mechanical support to the gold rod and thereby preserve the dimensional integrity of the diffusion zone during the lathe sectioning. The transparency of the epoxy used allowed optical alignment of the visually observed weld plane perpendicular to the axis of the lathe. The adjustable chuck on the precision lathe used for the sectioning operation facilitated such an alignment. A specially designed tool and a water-soluble lubricant were used to allow removal of 1- to 3-μ-thick sections in the region of the $Hf^{181}O_2$ tracer, which permitted sufficient accuracy in the measurement of the distance between the center of gravity of the Au^{195} distribution and the oxide marker. Where the radioactive marker was not present, 10- to 50-μ-thick sections were removed. Sections varying between 25 and 100 μ were removed in the Sb^{125} in Au specimens.

The epoxy proved far more useful than simply as a secure container for the specimen rod. In the presence of the lubricant, the epoxy chip became a sponge-like material that completely entrapped the gold chip in its volume. This effect permitted relatively simple collection of the tiny gold sections, and so made feasible the rapid processing of the many sections required to span the extremely large diffusion zones typical of the runs. Although epoxy and lubricant were present in the planchets along with the gold, they could be effectively eliminated by heating each planchet with a Bunsen flame until the epoxy and lubricant were reduced to a residue estimated to be no more than 0.2% of the weight of the gold. The weight measurement of the gold chip and carbonaceous residue, then, plus the measurement of the diameter of the diffusion zone with an optical comparator, allowed a determination of the thickness of each section.

In the Au^{195} in Au runs, the $Hf^{181}O_2$ distribution was determined by counting the oxide sections in both a low-background beta counter and the appropriate window of a conventional gamma-ray spectrometer. In the case of the Sb^{125}-Au^{195} in Au specimens, the Sb^{125}

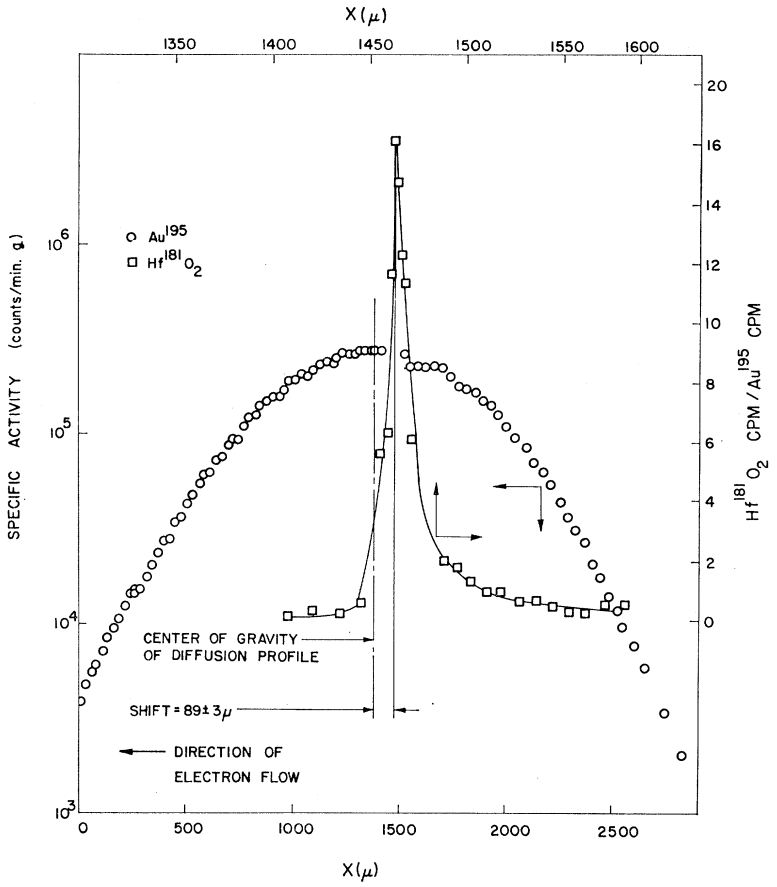

FIG. 2. Distributions of Au^{195} tracer and $Hf^{181}O_2$ marker in run 5 for $j=8.9\times10^3$ A/cm², $T=874$°C, $t=1.05\times10^6$ sec.

distribution was determined by the gamma spectrometer, using a window corresponding to the highest energy gammas of the Sb^{125} spectrum, while the Au^{195} distribution was determined by data from this high-energy window in conjunction with counts in a low-energy window corresponding to the Au^{195} K x rays.

D. Diffusion-Zone Temperature Measurement

The micro-optical pyrometer was merely used to monitor temperature fluctuations and estimate warm-up times. In addition, it was calibrated at the gold melting point, so that high-temperature runs could be safely attempted. The difference between the actual melting point temperature and the blackbody calibrated pyrometer reading at this point differed by about 130°C. An attempt was made to calibrate the entire usable range of the pyrometer by means of a gold resistivity temperature scale. Although this procedure provided temperature measurement accurate to 5 to 10°C for a given specimen, the varying emissivity from one specimen to another made this method totally inadequate.

In conventional diffusion coefficient determinations, the main uncertainty in the diffusion coefficient D is due to the uncertainty in the absolute temperature T. It is therefore desirable to minimize ΔT. This can be seen from the equations for D and $\Delta D/D$:

$$D=D_0e^{-Q/kT}, \tag{7}$$

$$\Delta D/D=(Q/kT)(\Delta T/T). \tag{8}$$

The quantity Q/kT is of the order of 20 for gold in the temperature range 850 to 1050°C. A 1°C uncertainty in T then gives about a 2% uncertainty in D. This very effect can be turned to advantage to determine the temperature scale in the present experiment, since measurement of the distribution of the Au^{195} tracer gives, in addition to the shift, a fairly precise value of the self-diffusion coefficient for gold. The measured value of the self-diffusion coefficients thus permits precise determination of the temperature scale, as discussed in Sec. III.

To permit use of such a diffusion coefficient temperature scale, accurate values of the self-diffusion coefficient had first to be determined. Since there were discrepancies in published values of this coefficient, a precise measurement of the temperature dependence of the diffusivity of Au^{195} in pure Au was first made.[14]

[14] H. M. Gilder and D. Lazarus, J. Phys. Chem. Solids **26**, 2081 (1965).

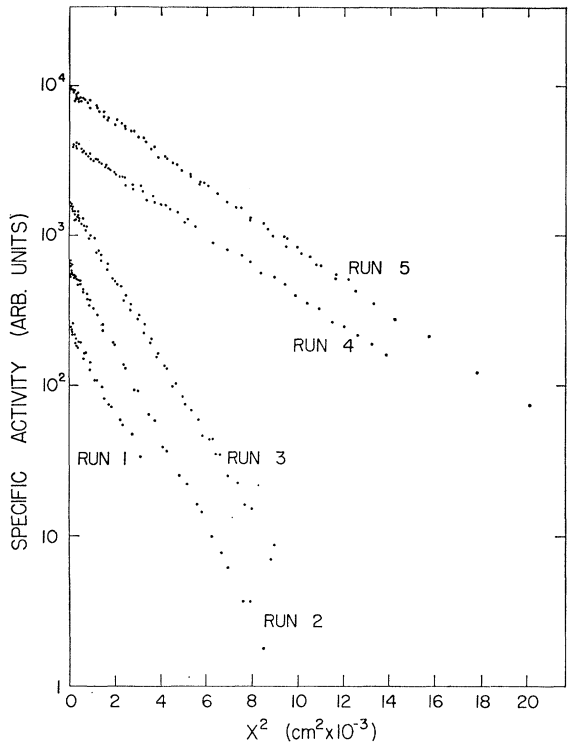

FIG. 3. Semilogarithmic plots of the Au^{195} diffusion profiles for runs 1–5. Points from both sides of the interface fit on a single Gaussian curve.

III. EXPERIMENTAL RESULTS

A. Shift of Gold Tracer

A total of five successful electromigration experiments were performed with specimens containing Au^{195} and $Hf^{181}O_2$ markers. The results are summarized in Table I, and a typical measurement is shown in Fig. 2, indicating the observed distributions of the two tracers. The run number indicates only the historical order of a particular measurement. Runs 2–5 were conducted with specimen rods cut from the same initial couple, while the rod used for run 1 was cut from another, earlier, couple containing a smaller amount of tracer, resulting in poorer counting statistics and reduced over-all accuracy for this first measurement.

Except for deliberate reversal of the specimen rods with respect to the cathode and anode in the specimen chamber to obviate any systematic errors from direction of flow of gold atoms through the oxide layer, all runs were conducted under essentially identical conditions. Current densities varied from 8.83×10^3 A/cm² at the lowest temperature (875°C) to 9.12×10^3 A/cm² at the highest (1018°C), while the corresponding diffusion times ranged from nominally 292 to 15 h.

In the tabulated results, the data are corrected for diffusion occurring during initial welding of the couple $[(Dt)^{1/2}\sim35\,\mu]$, and for warm-up time. Inasmuch as the continuous monitoring of a particular run was expressed in terms of optical pyrometer readings, the warm-up correction to the anneal time and temperature was accomplished by an iterative procedure; the sum of two-thirds of the initial transient time and the total time at constant temperature was taken as a first approximation to the time used with the measured slope of the Au^{195} diffusion profile in evaluating the gold self-diffusion coefficient. From this value, a first approximation to the actual temperature could be deduced against which the average value of optical pyrometer readings in the constant-temperature region could be calibrated. First-order diffusion coefficients were then calculated for the variable temperature region and a second approximation effective warm-up time calculated. One iteration was sufficient in all cases, since the first and second approximations to the time, and therefore the corresponding diffusion coefficients, differed by no more than 0.2%.

The shifts were determined by finding the centers of gravity of the gold tracers relative to the position of the hafnium-oxide markers, using a least-squares analysis. This procedure involved calculating the standard deviations of the residuals for a best-fit line to the data in both the "log-activity" and "x^2" directions as a function of diffusion-zone distance. The position at which the standard deviations reached a minimum was assumed to be the symmetry axis of the Gaussian diffusion profile. In all cases, not only was the center of gravity of the gold tracer distribution shifted toward the anode, but the distribution could be fit to a single Gaussian profile on both sides of the interface; except for a small systematically low plateau found near the peak on the cathode side in all runs, which

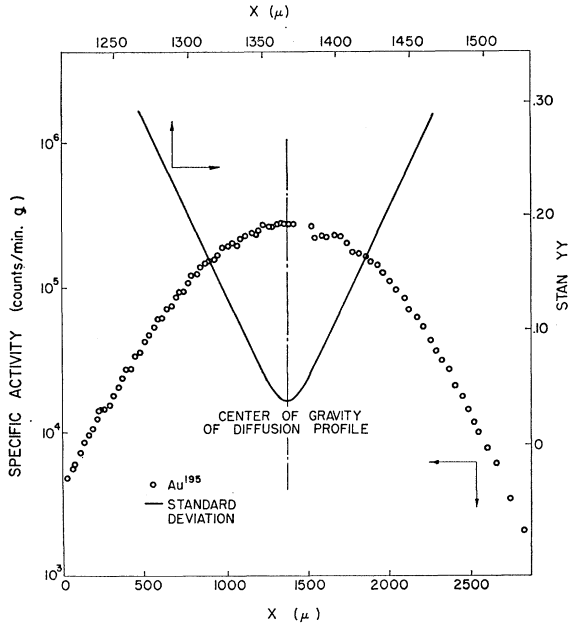

FIG. 4. Variation of the standard deviation Stan YY, with choice of center position for the Au^{195} distribution, for run 5.

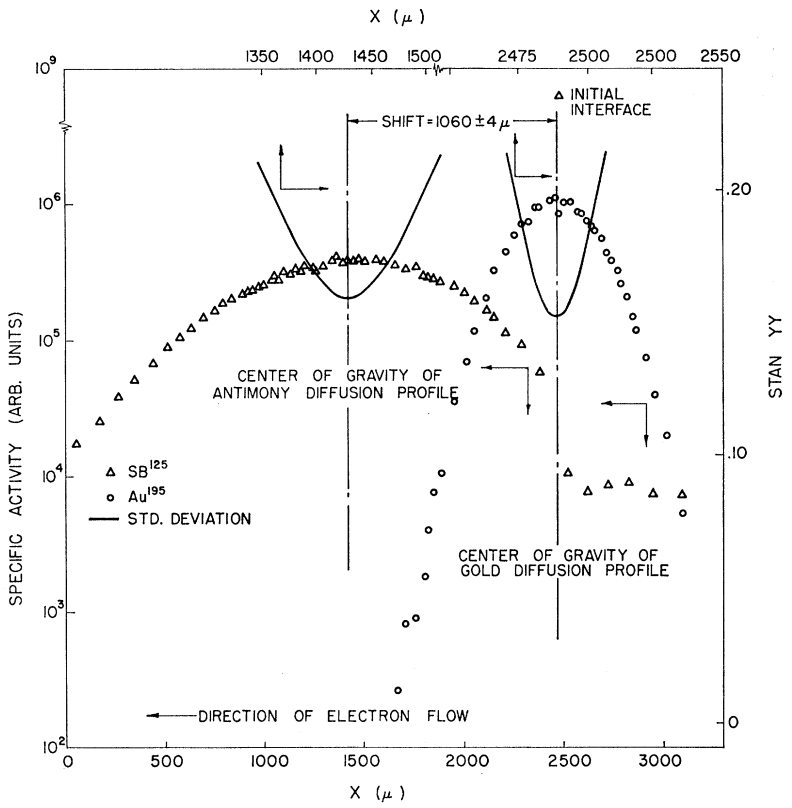

FIG. 5. Distribution of Sb^{125} and Au^{195} tracers for run 1Sb, and standard deviations for $j=9.1\times10^3$ A/cm^2, $T=1009$°C, and $t=2.5\times10^4$ sec.

had a negligible effect on the measured diffusivity, there was no evidence for any asymmetry in the Au^{195} distribution. The evident symmetry of the distribution of the gold tracer can be seen from the semilogarithmic plots shown in Fig. 3, where sections from both sides of the interface are seen to fit a single Gaussian profile. The symmetry of the curves of the standard deviations plotted against distance with respect to axes through the minima, as shown for a typical case in Fig. 4, is further evidence for symmetry of the gold distribution.

The distributions of $Hf^{181}O_2$ are determined in terms of the ratio of the $Hf^{181}O_2$ activity to the Au^{195} activity in the same section, since this procedure obviates scatter resulting from variation in thickness and weighing errors in the very tiny sections taken near the interface. The hafnium oxide tracer distributions in runs 1, 3, 4, and 5 were found to be symmetrical about the peak marking the initial interface, whereas in run 2 asymmetry was evident about the peak. The probable implications of this asymmetry will be discussed in Sec. IV.

The presence of the hafnium oxide was in all cases evident during the sectioning procedure, even without the continual monitoring of the actual tracer concentrations in successive sections. As there was slight misalignment of the specimen and lathe axes (~0.01 radian), the partial area of a visible dark layer was found to increase in magnitude and then decrease until it disappeared, as successive lathe sections were cut from the marker region. In addition, the mechanical behavior of these sections was markedly different from that of the pure-gold matrix; the sections containing minute amounts of the oxide tended to be removed as a powder by the lathe tool, while pure gold sections were always removed as coninuous fine chips.

B. Shift of Antimony Tracer

Two successful electromigration experiments were carried out with specimens containing Sb^{125} and Au^{195} tracers, the latter serving as a temperature indicator and fiducial marker with respect to which the antimony shift was observed. Both experiments were conducted with specimen rods cut from the same initial couple and run under essentially identical conditions. Current densities varied from 8.24×10^3 A/cm^2 at the lower temperature (853°C) to 9.10×10^3 A/cm^2 at the higher (1009°C), while the corresponding diffusion times ranged from nominally 24 to 6 h.

The raw data for one run are given in Fig. 5 showing the actual measured distributions of Sb^{125} and Au^{195} in the specimen. The effective anneal times and anneal temperatures were determined by the iterative procedure previously described, while the shifts were determined by finding the centers of gravity of the antimony tracers relative to the centers of gravity of the Au^{195} tracers. The centers of gravity were determined by the least-squares analysis mentioned earlier,

and were shifted toward the anode. In both cases, the distribution of the gold tracers could be fit to a single Gaussian profile on both sides of the interface, whereas the antimony tracers showed nearly Gaussian behavior on the anode side of the interface but anomalous behavior at the initial interface (an extremely high peak) and on the cathode side (very slow fall-off of specific activity with increasing distance away from the interface). The probable implications of these anomalies will be discussed in Sec. IV.

C. Discussion of Experimental Accuracy

1. Measurement of Gold Shift

In the case of the gold shifts, the experimental uncertainty in the measurement of the displacement of the center of gravity with respect to the oxide marker can be conveniently divided into two parts: the uncertainty in the position of the center of gravity as reflected by the standard deviation in the x direction and the uncertainty in the position of the $Hf^{181}O_2$ peak as determined by the thickness of the section in which it was localized.

The factors influencing the standard deviation are the uncertainties in the section weights and count rates. The random error in reading the precision balance employed in the differential weight measurement of the sections is estimated to be $\pm 3\times 10^{-5}$ g. As section weights in the pure gold run averaged about 4×10^{-3} g outside of the oxide region, the weight error was of the order of 1%. The extremely thin oxide sections averaged about 3×10^{-4} g but were determined to better than the indicated 10% uncertainty by scaling the count rates of these sections to the pure gold specific activities from sections adjacent to the marker region. As the marker distribution extended over a small region compared to the characteristic dimension of the gold Gaussian profile, and was always close to the peak, the estimated uncertainty in the weights of the thin sections is about 3%. This latter random error, then, probably contributes about ± 0.6 μ to the shift (0.7 mg$\simeq$10 μ), while the errors in weighing the heavy sections contribute about ± 0.2 μ as well. The total contribution from these two sources is then of the order of ± 0.7 μ.

The other factor affecting the standard deviation is the count-rate accuracy. Count rates were determined in runs 2–5 to about 1%, whereas run 1, being a very low-activity specimen, had count rates accurate to about 2%. The specific activities were then determined to within about 2–3% and the natural logarithms of specific activities to better than 1–2%. These two estimates are in agreement with the x-direction scatter of from 0.7 to 1.5 μ, encompassing all pure gold runs, as determined by the least-squares analysis.

The section thicknesses in which the $Hf^{181}O_2$ maxima were localized averaged about 2 μ in runs 2–5 and 10 μ in run 1. This contribution gives an additional uncertainty in the shift of ± 1 μ in runs 2–5 and ± 5 μ in run 1. The total uncertainty in the measured shifts, then, is about ± 2 μ in runs 2–5 and ± 5 μ in run 1.

2. Temperature Measurement

The effective temperature at which electromigration occurred was calculated on the basis of the least-squares slopes of the diffusion profiles portrayed in a semilogarithmic plot and the diffusion occurring during the weld of the initial couple. Thus, the significant quantities affecting the uncertainty in the temperature are the standard deviation of the slope and the uncertainty in the weld-penetration depth of the gold tracer.

If we let

m = the least-squares slope of the diffusion profile,

t_r = the time during which electromigration took place,

D_r = the diffusion coefficient appropriate to the period of the electromigration experiment,

t_w = the effective time appropriate to the weld process, and

D_w = the diffusion coefficient appropriate to the time of weld formation,

then

$$m=1/4(D_r t_r+D_w t_w), \tag{9}$$

and

$$x_w^2\equiv 4D_w t_w. \tag{10}$$

Between Eqs. (9) and (10) we find

$$4D_r t_r=1/m-x_w^2. \tag{11}$$

Taking differential increments of both sides of (11):

$$\Delta D_r/D_r-\Delta t_r/t_r=(\Delta m/m+2x_w m\Delta x_w)/(1-mx_w^2), \tag{12}$$

where the signs of the differential quantities have been purposely chosen to maximize $\Delta D_r/D_r$. As x_w^2 was determined experimentally to fall between 36×10^{-6} cm^2 and 72×10^{-6} cm^2, and m was found to range from -250 to -600 cm^{-2}, the maximum possible value for the quantity mx_w^2 is 0.04. Since the quantity $\Delta t_r/t_r$ is in all cases of the order of 0.1% for the relatively long pure-gold runs, Eq. (12) can be written as:

$$\Delta D_r/D_r=1.04(\Delta m/m+2x_w m\Delta x_w). \tag{13}$$

If we take x_w and Δx_w to be 72 μ and 12 μ, respectively, then the maximum value of the second term on the right-hand side of Eq. (13) is 10^{-2}. In addition, for runs 2–5, $\Delta m/m$ varies between 0.3 and 0.8%, so that $(\Delta D_r/D_r)_{\max}$ varies between 1.4 and 1.9%. From Eq. (8) and assuming a conservative value of Q/kT of 17, $(\Delta T/T)_{\max}$ varies between 0.08 and 0.11%. For $T=1300$°K, $\Delta T_{\max}=\pm 1.4$°C. For run 1, $\Delta m/m$ has the value 2×10^{-2}, so that in this case $(\Delta D_r/D_r)_{\max}$ is about 3.1%. This implies a value of $(\Delta T/T)_{\max}$ of 0.18%. For the first run, then, $\Delta T_{\max}=\pm 2.3$°C. The temperature uncertainty is therefore conservatively estimated at ± 2°C for all gold runs.

TABLE II. Parameters describing the electromigration of the Au^{195} ion in gold.

Run No.	v (cm/sec)	j (A/cm²)	v/j (cm³/sec A)	ρ ($\mu\Omega$ cm)	e^* (units of e)	$\Delta\rho_0^*/c$ [$\mu\Omega$ cm/(% defect)]
1	6.5×10^{-8}	9.12×10^{3}	7.1×10^{-12}	12.55	11 ±1.6	1.2±0.3
2	4.8×10^{-8}	8.15×10^{3}	5.9×10^{-12}	12.69	7.6±0.8	1.2±0.3
3	6.6×10^{-8}	9.11×10^{3}	7.3×10^{-12}	12.84	8.4±0.4	1.2±0.3
4	1.7×10^{-8}	8.83×10^{3}	1.9×10^{-12}	11.44	8.8±0.5	1.2±0.3
5	8.5×10^{-9}	8.87×10^{3}	9.6×10^{-13}	10.83	9.2±0.5	1.2±0.3

The previous analysis pertains to the temperature measurement in the antimony runs as well as the pure-gold runs; since the couple was welded under identical conditions to that in the pure-gold experiment, and $\Delta t_r/t_r$ is again negligible compared to other quantities, Eq. (12) may be utilized to arrive at $(\Delta T/T)_{\max}$. For run 1Sb, m and "Δm" were 1307 cm^{-2} and ±14 cm^{-2}, respectively, giving a value of $(\Delta D_r/D_r)_{\max}$ of 4.0%, and $(\Delta T/T)_{\max}=0.24\%$. For run 2Sb, "$m$" and "$\Delta m$" were 3318 cm^{-2} and ±33 cm^{-2}, respectively, giving $(\Delta D_r/D_r)_{\max}=7.9\%$, and $(\Delta T/T)_{\max}=0.42\%$. For $T\approx1300$°K, the temperature uncertainties in the antimony runs are then conservatively estimated to be ±3 and ±5°C for runs 1Sb and 2Sb, respectively.

3. *Current Density Measurement for Gold and Antimony Shifts*

By calibrating the ammeter in the dc power supply and connecting the meter terminals to a strip-chart recorder so that a continuous record of the current could be kept, the average value of the current could be determined to within ±1%. As the diameter of the specimen rods could be measured to better than one part in five hundred, the total uncertainty in the current density is estimated to be ±1.4%.

4. *Measurement of Antimony Shift*

With regard to the antimony shifts, the uncertainty in the shift is simply the sum of the standard deviations in the x direction for both the antimony and gold Gaussian profiles. The factors influencing the standard deviations were determined to comparable degrees of accuracy in both the pure gold and antimony experiments. For both runs, the standard deviation for the Sb^{125} profile was about ±3 μ while that for the Au^{195} profile was ±2 μ. The shift of the antimony with respect to the gold is therefore given to an accuracy of ±4 μ.

IV. DISCUSSION AND INTERPRETATION OF DATA

A. Electromigration of Gold

1. *Comparison of Data with Nernst-Einstein Relation*

The Nernst-Einstein relation as expressed in Eq. (5) can be cast in a form showing the explicit dependence of the ionic drift velocity v on the current density j and the effective ionic charge e^*. If we assume that the total force on the ion due to its interaction with the electron system and the external electric field ϵ can be expressed as

$$\mathfrak{F}(x)=e(x)\epsilon, \tag{14}$$

where $e(x)$ is a spatially varying effective charge, then the change in barrier height for self-diffusion ΔV can be written

$$\Delta V=\int_0^{\lambda/2}\mathfrak{F}(x)\,dx=\epsilon\int_0^{\lambda/2}e(x)\,dx. \tag{15}$$

It should be emphasized that the total force defined by Eq. (14) is composed of two opposing forces which tend to create a drift in the motion of the diffusing atoms; the electric field across the sample tends to drive the positive gold ions toward the cathode, while the direct momentum exchange with the moving electron stream tends to cause motion in the opposite direction, toward the anode. In all cases the observed motion of the center of gravity of the Au^{195} distribution is shifted toward the anode, indicating that the major part of the total force on the ion arises from momentum exchange with the conduction electrons.

The average value of $e(x)$ over the jump distance λ can be defined as

$$e^*=(2/\lambda)\int_0^{\lambda/2}e(x)\,dx. \tag{16}$$

Substituting Eq. (16) in Eq. (15)

$$\Delta V=e^*\epsilon\lambda/2, \tag{17}$$

Eq. (5) then becomes

$$v/j=(e^*/k)\rho D/T. \tag{18}$$

Taking the natural logarithm of both sides of the last equation, and differentiating with respect to reciprocal temperature, we obtain

$$\frac{\partial}{\partial(1/T)}\ln(v/j)=\frac{\partial}{\partial(1/T)}\ln(e^*/k)+\frac{\partial}{\partial(1/T)}\ln(\rho/T)-Q/k. \tag{19}$$

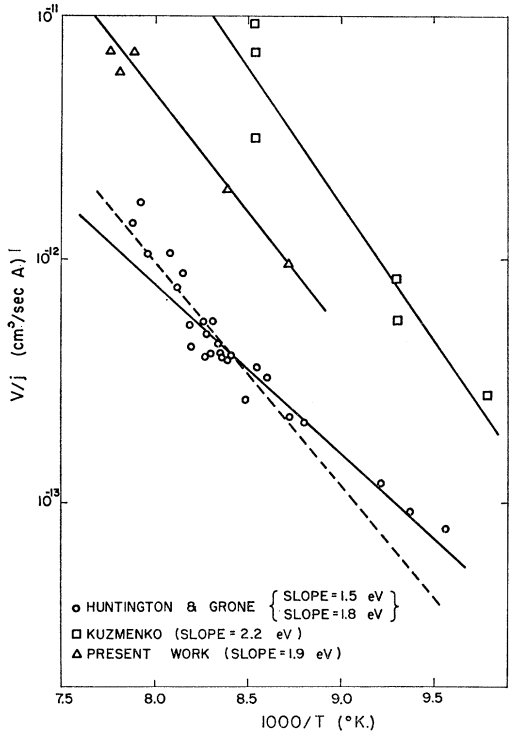

FIG. 6. Present results compared with previous measurements on semilogarithmic plot as function of reciprocal absolute temperature.

If e^* is temperature-independent, and the quantity $|\partial/\partial(1/T)\ln(\rho/T)|$ is small compared to $|Q/k|$, then a plot of $\ln(v/j)$ versus $1/T$ should be a straight line with a slope of 1.83 eV, the self-diffusion activation energy for gold. In fact, by inspection of Table II and Fig. 6, the effective charge, within experimental uncertainty, is temperature-independent, and the slope of the best-fit line to the $\ln(v/j)$ versus $1/T$ data, excluding the 1007°C point, has a slope of 1.93 eV. In addition, the quantity $\partial/\partial(1/T)\ln(\rho/T)$ has the value -0.05 eV, so that the observed value of the activation energy is (1.9 ± 0.1) eV, in excellent agreement with the precisely determined value of (1.83 ± 0.01) eV for self-diffusion in gold.[14] To within the experimental uncertainty, then, the Nernst-Einstein relation is apparently obeyed.

2. *Shape of the* $Hf^{181}O_2$ *Distribution*

The only run that showed marked asymmetry of the hafnium oxide distribution was run 2. As shown in Fig. 7, it is evident that there is a plateau on the anode side, and a fall-off of activity on the cathode side within a distance of the order of 20 μ. Since there was visual evidence for misalignment of the specimen relative to the lathe axis as sectioning proceeded through the initial interface, the cathode-side portion of the distribution can easily be explained in terms of a misalignment angle of the order of 0.01 radian. However, misalignment during sectioning would lead to a symmetrical "spread-out" of the distribution as noted in the other specimens. The plateau occurs on the anode side, where vacancies are in excess, since the direction of the vacancy current must be from anode to cathode, opposite to the direction of drift of the atoms. Some of the vacancies may precipitate at pores on the anode side and would not contribute to the shift. The presence of the plateau on the anode side is then suggestive of void formation in the specimen, and is consistent with the fact that the observed shift was anomalously small in this case. The area determined by the boundary of the plateau and the reflected symmetrical portion is proportional to the fraction of the hafnium oxide enveloped by the pores. This explanation seems plausible for basically two reasons: First, the hafnium oxide is so poorly matched to the gold lattice that the oxide particles act as efficient sites for vacancy precipitation, which serves to relieve the local stresses in the vicinity of the oxide; and secondly, the formation of pores by vacancy precipitation would decrease the number of vacancy-tracer interchanges and result in a smaller shift of the tracer, in agreement with the observed low "v/j" value relative to the best-fit line for run 2. Void formation is nearly always observed in Kirkendall experiments,[15] where vacancy currents are induced by chemical concentration gradients rather than by the electric potential gradient operating here, so the possibility that part of the shift may be masked by porosity in the present experiment is hardly surprising.

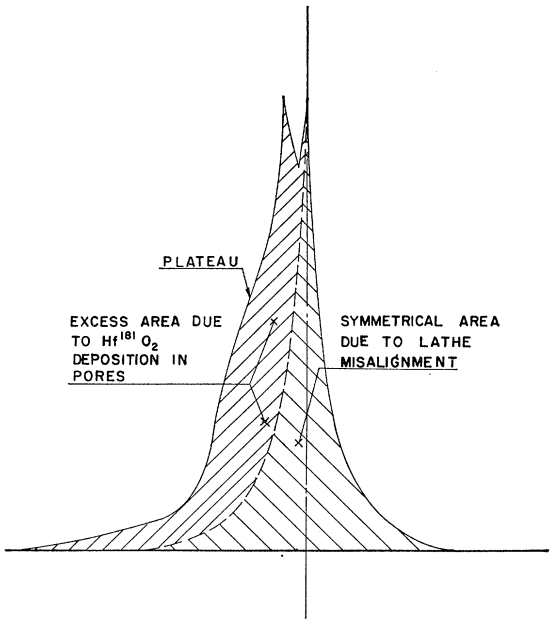

FIG. 7. Asymmetrical $Hf^{181}O_2$ distribution for run 2.

[15] R. S. Barnes and D. J. Mazey, Acta Met. 6, 1 (1958); R. W. Balluffi and B. H. Alexander, J. Appl. Phys. 23, 1237 (1952).

3. Comparison with Previous Results

Figure 6 shows the present data and those of Huntington and Grone and of Kuzmenko, plotted on the same graph. The straight line from Huntington and Grone represents their data taken with a current of 30 A. The data points shown are taken with a current of 60 A. In both cases the lower temperature points were equally weighted although their accuracy was relatively lower than the others, and may have unduly biased the fit. The slope of the line is 1.5 eV and, even within the scatter of their data, it appears that this value is a bit too low compared to the precise value of 1.83 eV. On the other hand, if their data are analyzed excluding the low-temperature points, the remaining points give a best-fit activation energy of 1.8 eV. This adjustment brings their data into excellent agreement with the values 1.9 eV (from electromigration data) and 1.83 eV (from precise self-diffusion data) obtained in the present experiment. A best-fit line to Kuzmenko's data gives an activation energy of 2.2 eV, but from the scatter of his data, it is apparent that this activation energy could easily overlap the present value, as well.

Although the three sets of data appear to be in essential agreement on the value for the activation energy, there is a considerable difference between the actual magnitudes of the v/j values, even taking account of the experimental uncertainties in each experiment. Kuzmenko's values are a factor of 3 to 4 times larger than the present results and Huntington and Grone's factor of 3 to 4 lower. As Kuzmenko measured the tracer shift after breaking open the couple welded only during the time of electromigration, the actual temperature in the zone which encompassed this presumably extremely porous region at the weld could have been higher than the temperature reported, accounting for the consistently higher velocities obtained. On the other hand, if the weld were sufficiently sound to realize a well-defined temperature in the region of diffusion, then the act of breaking open the specimen could very likely have caused marked distortion of the diffusion zone, and thereby exaggerated the actual shift.

With regard to the lower v/j values of Huntington and Grone, it should be realized that the mobilities measured in their experiment are dependent on the possibility of lattice distortion in the vicinity of the scratch marks used to follow the atomic motion. Although there is the possibility of lattice distortion in this experiment because of the creation of additional atomic planes on the anode side and annihilation of planes on the cathode side, the measurement of the shift relative to the hafnium oxide marker would obviate errors due to this effect, since the marker would "take up" this distortion, as well. In addition, the shift as measured in the Huntington and Grone experiment gives a mobility that depends, not on the mass flow at the marker location as it does in the present experiment, but on the dimensional changes between the marker in question and a fiducial marker in the cold region of the specimen. If these dimensional changes are isotropic, as later evidence[8] indicates, then Huntington and Grone's mobility should be a third smaller than ours. This effect should then tend to increase the Huntington and Grone shifts relative to those obtained in the present experiment.

In addition to calculating an activation energy for self-diffusion, the data lend themselves to an estimate of the effective charge e^* on the activated gold ion-vacancy complex, and a measurement of the electrical resistivity of this complex, as well. By using Eq. (18) and values of the bulk resistivity of gold, as well as the measured diffusion coefficients for each electromigration run, the effective charge e^* was found to be independent of temperature within the experimental uncertainty, as shown in Table II. Averaging e^* over runs 1, 3, 4, and 5, we obtain $e^*=(9\pm1)e$. Huntington and Grone, on the other hand, found a variation of e^* of from $5e$ at 1000°C to $8e$ at 800°C. However, this temperature dependence appears to be the result of their using a value of 1.8 eV for the self-diffusion activation energy for gold rather than their own quoted best-fit value of 1.5 eV. This, then, gives them a temperature dependence of e^* of the form $e^*=e_0^*\exp(0.3\text{ eV}/kT)$. On the basis of the present data and the same method of calculation employed by Huntington and Grone, it appears that the effective charge on the ion is actually temperature-independent.

In the framework of Fiks' formulation,[3] the ionic mobility v/j can be expressed as

$$v/j=\rho D/kT[e(1-\Delta\rho_0^*/c\rho)]=(\rho D/kT)e^*, \quad (20)$$

where $\Delta\rho_0^*$ is the residual resistance connected with the scattering of electrons at the activated gold ion-vacancy complex, and c is the atomic fraction of such scattering centers. If Eq. (20) is solved for $\Delta\rho_0^*/c$ and a temperature-averaged value of $\rho=11.9$ $\mu\Omega$ cm assummed, the resistivity of these scattering centers is estimated to be (1.2 ± 0.3) $\mu\Omega$ cm/(% defect). This value is in agreement with Huntington and Grone's value of 2 $\mu\Omega$ cm/(% defect) and comparable to theoretical estimates for the specific resistivities of other point defects.[16]

B. Electromigration of Antimony in Gold

In both antimony runs, there were consistent anomalies in the Sb^{125} distributions. The high, narrow peak at the initial interface, in both cases, is presumably attributable to trapping of most of the antimony tracer at the initial interface due to the relatively low solubility of antimony in gold, and the possibility of oxide formation. In addition, the anomalously slow fall-off of the antimony distribution on the cathode side of the

[16] P. Jonenburger, Appl. Sci. Res. **B3**, 237 (1953).

TABLE III. Parameters describing the electromigration of the Sb^{125} ion in gold.

Run No.	Shift, Δx (μ)	Current, I (A)	Time, t (sec)	Temp., T (°K)	j (A/cm²)	v/j (cm³/sec A)	e^* (units of e)	$\Delta\rho_0^*/c$ [$\mu\Omega$ cm/(% defect)]
1SB	1060±4	672±1	2.569×10^4	1282±3	9.10×10^3	4.54×10^{-10}	140±40	18±6
2SB	674±4	634±2	8.854×10^4	1126±5	8.24×10^3	9.24×10^{-11}	140±40	18±6

interface is, by the same token, attributable to the tracer distribution after welding being driven by the electric field back to the initial interface, apparently being partially reflected by the excess antimony barrier there. On the anode side, there appears to be a slight bulge in the Sb^{125} distribution between the initial interface and the peak of the Sb^{125} Gaussian. The asymmetry is not nearly as exaggerated as on the cathode side, since the tracer is driven away from the barrier on the anode side and toward the barrier on the cathode side.

Although only two shifts were measured for the electromigration of antimony in gold, there is sufficient information to estimate the effective charge and specific resistivity of the activated antimony ion-vacancy complex, as well as the impurity diffusion coefficient. If we assume that the data obey the Nernst-Einstein relation, and in addition that the effective charge is temperature-independent (presumably a good assumption on the basis of the pure-gold data), we then have the following relation for the ratio of the antimony mobilities at two different temperatures T_1 and T_2:

$$(v/j)T_1/(v/j)T_2=\rho(T_1)/\rho(T_2)(T_2/T_1)\times D_{Sb}(T_1)/D_{Sb}(T_2). \quad (21)$$

In this equation, $D_{Sb}(T)$ is the diffusion coefficient of antimony in gold, and $\rho(T)$ is the bulk resistivity of gold. In addition, $D(T)$ can be expressed as

$$D_{Sb}(T)=(D_0)_{Sb}e^{-Q_{Sb}/kT}. \quad (22)$$

Using the values of v/j listed in Table III, we find that $D_{Sb}(1282°K)/D_{Sb}(1126°K)=4.7$ and $Q_{Sb}=1.2$ eV. This value of Q_{Sb} appears to be low compared to the activation energy for antimony diffusion in silver[17] and copper[18] but the value calculated here on the basis of just 2 points is probably uncertain to within 20–40%. The diffusion coefficient at either 1282 or 1126°K can be estimated by using the above value of $D_{Sb}(1282°K)/D_{Sb}(1126°K)$ in conjunction with the following relations:

$$m(T_1)=\tfrac{1}{4}(D_{Sb}(T_1)t_1+D_{Sb}(T_w)t_w], \quad (23)$$

and

$$m(T_2)=\tfrac{1}{4}[D_{Sb}(T_2)t_2+D_{Sb}(T_w)t_w]. \quad (24)$$

Solving Eqs. (23) and (24) we obtain $D_{Sb}(1282°K)=3\times10^{-8}$ cm²/sec. The weld penetration distance of the antimony tracer cannot be ignored in the solution of Eqs. (23) and (24) since it is an appreciable fraction of the antimony mean-square diffusional penetration distance during electromigration. Using the values of ρ and v/j appropriate to $T=1282°K$, Eq. (20) gives a value of $140e$ for the effective charge on the antimony ion-vacancy complex. Equation (20) can then be used to yield a value for $\Delta\rho/c$ of 18 $\mu\Omega$ cm/(% defect) for the activated complex. This value seems entirely reasonable on the basis of the value for $\Delta\rho/c$ of 7.26 $\mu\Omega$ cm/(at.%) and 5.45 $\mu\Omega$ cm/(at.%) for antimony in silver and copper,[19] respectively. The activated complex presumably should have a higher specific resistivity than that of the corresponding normal impurity ion in the host lattice.

As seen in Tables II and III, the mobility of the antimony ion is some 1 to 2 orders of magnitude larger than that of the solvent gold atoms, and the shift of the antimony tracer is actually about 50% greater than the mean-square diffusional penetration distance of the antimony. It would then appear that electromigration techniques could possibly be adapted as a practical method for purifying metals.

ACKNOWLEDGMENTS

The authors wish to express their sincere thanks to Professor H. B. Huntington for several enlightening discussions relative to electromigration phenomena, to William Mock for assistance in taking some of the data, to Dr. R. Meyer and Dr. L. Slifkin for communicating their technique for use of $Hf^{181}O_2$ markers, and to F. Wise, W. Craig, and Bud Dittman for invaluable help in critical machining operations.

[17] E. Sonder, L. Slifkin, and C. T. Tomizuka, Phys. Rev. **93**, 970 (1954).

[18] M. C. Inman and L. W. Barr, Acta Met. **8**, 112 (1960).

[19] J. O. Linde, Ann. Physik **15**, 219 (1932).